AMERICAN SOCIETY FOR MICROBIOLOGY | Molecular and Cellular Biology®

RESEARCH ARTICLE

The Upregulation of HAS2-AS1 Relates to the Granulosa Cell Dysfunction by Repressing TGF-β Signaling and Upregulating HAS2

Yungai Xiang,[a] Guo Yu,[a] Yuxia Song,[a] Yan Li,[a] Lanlan Cheng,[a] Pengfen Li,[a] Le Zhang,[a] Meng Wang,[a] Li Tan[a]

[a]Department of Reproductive Medicine, The Second Affiliated Hospital of Zhengzhou University, Zhengzhou, Henan, China

ABSTRACT HAS2 antisense RNA 1 (HAS2-AS1) is a long noncoding RNA that has increased expression in mature granulosa cells (GCs) and contributes to cumulus expansion by regulating HAS2 expression. However, the roles of HAS2-AS1 during the pathological process of polycystic ovary syndrome (PCOS) are still unclear. This study investigated the roles of HAS2-AS1 in patients with PCOS. Here, a significant upregulation of HAS2-AS1 was found in the primary GCs from patients with PCOS, which was positively correlated with the level of the protein HAS2. The knockdown of HAS2 restored the upregulation of HAS2-AS1 in promoting migration but could not restore the effects of HAS2-AS1 overexpression in promoting proliferation and repressing apoptosis. Transforming growth factor β (TGF-β) upregulated HAS2-AS1 levels, while HAS2-AS1 functioned as a feedback inhibition factor repressing TGF-β signaling by inhibiting TGF-β receptor type 2 (TGFBR2) expression. HAS2-AS1 bonded with EZH2 and guided the polycomb complex 2 to the TGFBR2 promoter region. HAS2-AS1 overexpression induced H3K27 hypermethylation in the TGFBR2 promoter region and then repressed TGFBR2 transcription in KGN cells and primary GCs. In conclusion, we identified for the first time that HAS2-AS1 is upregulated in patients with PCOS and represses TGF-β signaling via inducing TGFBR2 promoter region hypermethylation, which allowed us to explore the pathological processes of PCOS.

KEYWORDS polycystic ovary syndrome, granulosa cell, long noncoding RNA, HAS2-AS1, H3K27me3

Polycystic ovary syndrome (PCOS) is a common metabolic and reproductive disorder affecting 6% to 20% of women of reproductive age (1, 2). Patients with PCOS usually have complex phenotypes, including reproductive comorbidities (irregular periods, abnormal folliculogenesis, ovulatory dysfunction, and infertility) and metabolic disorders (insulin resistance, elevated androgens, and cardiovascular disease). The etiology of PCOS is complex and includes genetic, environmental, and epigenetic factors (3). Granulosa cells (GCs) are a group of somatic cells which form a single layer around the oocytes and provide nutrients and growth regulators for the oocytes (4). Emerging evidence indicates that GCs in PCOS patients have abnormal proliferation (5). Furthermore, these GCs have been found more sensitive to some hormones, like follicle-stimulating hormone (FSH), indicating that the dysregulation of GCs may contribute to the pathophysiological processes of PCOS (6, 7).

Owing to the findings of high-throughput sequencing, most of the human genome is transcribed into non-protein-coding RNAs (ncRNAs), which are mainly divided into long ncRNAs (lncRNAs) and small ncRNAs (microRNA, PIWI-interacting RNA, and small nucleolar RNA). Emerging evidence indicates that some of the ncRNAs play an important regulatory role for maintaining healthy ovarian function, and abnormal expression of ncRNAs has been found to be related to the pathogenesis of PCOS (8, 9).

HAS2 antisense RNA 1 (HAS2-AS1) is located on chromosome 8q24.13 and is transcribed from the opposite strand of the HAS2 gene locus, which was first described in 2005 (10). The

Address correspondence to Li Tan, tanli996@yahoo.com.

The authors declare no conflict of interest.

Received 21 March 2022
Returned for modification 13 April 2022
Accepted 18 July 2022
Published 8 August 2022

HAS2-AS1 transcript consists of four exons, and the presence of an alternative splicing site inside exon 2 allows the generation of two splicing isoforms of different lengths (10, 11). These two isoforms show perfect complementarity with a region starting about 70 bp from the presumed transcription initiation site of human HAS2, allowing HAS2 mRNA and HAS2-AS1 natural antisense to form a heteroduplex (11, 12). Initially, HAS2-AS2 was identified as a suppressor for hyaluronan synthase 2 (HAS2) expression and of U2OS cell proliferation (10). However, in 2011, HAS2-AS1 was found to be a positive regulator for HAS2 expression by forming a double-strand RNA with HAS2 mRNA, which further stabilized HAS2 mRNA in renal proximal tubular epithelial cells (12). Additionally, HAS2-AS1 also works in *cis*, regulating HAS2 transcription by altering the chromatin structure around the HAS2 proximal promoter via O-GlcNAcylation and acetylation (13).

In reproduction systems, the level of HAS2-AS1 is very low in immature GCs but is increased in mature GCs (14). Meanwhile, HAS2-AS1 modulates cumulus expansion and migration by regulating HAS2 expression (14). HAS2-AS1 is overexpressed in ovarian cancer and promotes cancer cell proliferation and migration (15). However, the roles of HAS2-AS1 during the pathogenesis of PCOS are unknown.

The transforming growth factor β (TGF-β) signaling pathway plays key roles in maintaining the normal physiological conditions of the placenta, and the TGF-β signaling is dysregulated in patients with PCOS (16, 17). Meanwhile, the interaction between HAS2-AS1 and the TGF-β signaling pathway has been partially reported. For example, HAS2-AS1 has been identified to be upregulated by TGF-β in renal proximal tubular epithelial cells (12). HAS2-AS1 has been found positively correlated to the expression of TGF-β-induced epithelial-mesenchymal transition markers in breast cancer (18). However, whether HAS2-AS1 is regulated by the TGF-β signaling pathway in GCs is still unknown.

Additionally, it has been identified that HAS2-AS1 is involved in regulating TGF-β signaling in breast cancer cells (18), phosphatidylinositol 3-kinase (PI3K)/Akt in glioma cells (19), and NF-κB signaling in aortic smooth muscle cells (20). Meanwhile, these three signaling pathways are usually dysregulated in patients with PCOS (21, 22). However, genes usually play roles in a cell type-specific manner. So, whether HAS2-AS2 is related to these pathways in granulosa cells is unknown.

In the present study, GCs were isolated from 76 patients with PCOS and 18 healthy controls. The level of HAS2-AS1 was examined. The involvement of HAS2-AS1 in TGF-β, PI3K/Akt, and NF-κB signaling pathways was examined in granulosa cells. HAS2-AS1 was confirmed to be a multifunctional lncRNA that regulates mRNA degradation and histone methylation.

RESULTS

HAS2-AS1 is overexpressed in patients with PCOS and positively correlated with HAS2 protein level. To explore whether HAS2-AS1 is involved in the pathogenesis of PCOS, the HAS2-AS1 level was examined by reverse transcription-quantitative PCR (RT-qPCR) in the GCs from 76 patients with PCOS and 18 healthy controls. As shown in Fig. 1A, the level of HAS2-AS1 was significantly upregulated in the GCs from patients with PCOS compared with healthy controls. It has been reported that HAS2-AS1 regulates HAS2 expression in U2OS cells and renal proximal tubular epithelial cells through distinct mechanisms (10, 12). To understand whether HAS2-AS1 regulates HAS2 expression in GCs, we examined the protein level of HAS2 by immunoblotting analysis of GCs from patients with PCOS and controls. We observed that the HAS2 protein level was significantly upregulated in GCs from patients with PCOS (Fig. 1B and C) and positively correlated with the HAS2-AS1 RNA level (Fig. 1D), suggesting that HAS2-AS1 may regulate HAS2 expression in GCs.

HAS2-AS1 promotes GC proliferation and migration and inhibits apoptosis through regulating HAS2. To explore the biological function of HAS2-AS1 in GCs, HAS2-AS1-overexpressing KGN cells were generated. In addition, HAS2-AS1 was knocked down in KGN cells by small interfering RNA (siRNA) transient transfection. As shown in Fig. 2A, the HAS2-AS1 level increased to 8.26-fold in the HAS2-AS1 overexpression cells and was reduced to 12.5% by siHAS2-AS1. Immunoblotting results showed that HAS2 protein level was upregulated in HAS2-AS1-overexpressing cells and downregulated in HAS2-AS1 knockdown cells, indicating that HAS2-AS1 positively controlled HAS2 expression (Fig. 2B).

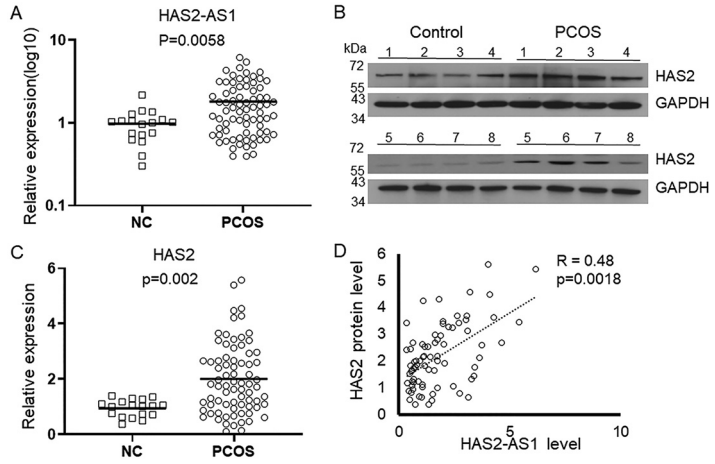

FIG 1 HAS2-AS1 is overexpressed in patients with PCOS and positively correlated with HAS2 protein level. (A) Primary granulosa cells were isolated from 76 PCOS patients and 18 healthy controls (NC). Total RNAs were extracted, and the level of HAS2-AS1 was quantified by RT-qPCR. Results were analyzed by using an unpaired *t* test, and a *P* value of <0.05 was considered significant. (B) The protein level of HAS2 was examined by immunoblotting. (C) The relative HAS2 expression levels were quantified by using Image J, and the results were analyzed with an unpaired *t* test. A *P* value of <0.05 was considered significant. (D) The correlation between HAS2-AS1 RNA level and HAS2 protein level in patients with PCOS was analyzed by $\chi 2$ analysis. A *P* value of <0.05 was considered significant.

Since GCs provide nutrients and growth regulators for oocytes, maintenance of a healthy physiology condition is necessary for oocyte development (4). In addition, GCs have been reported to migrate in response to human chorionic gonadotropin, which is important for the formation of the corpus luteum (23, 24). To understand whether HAS2-AS2 regulates

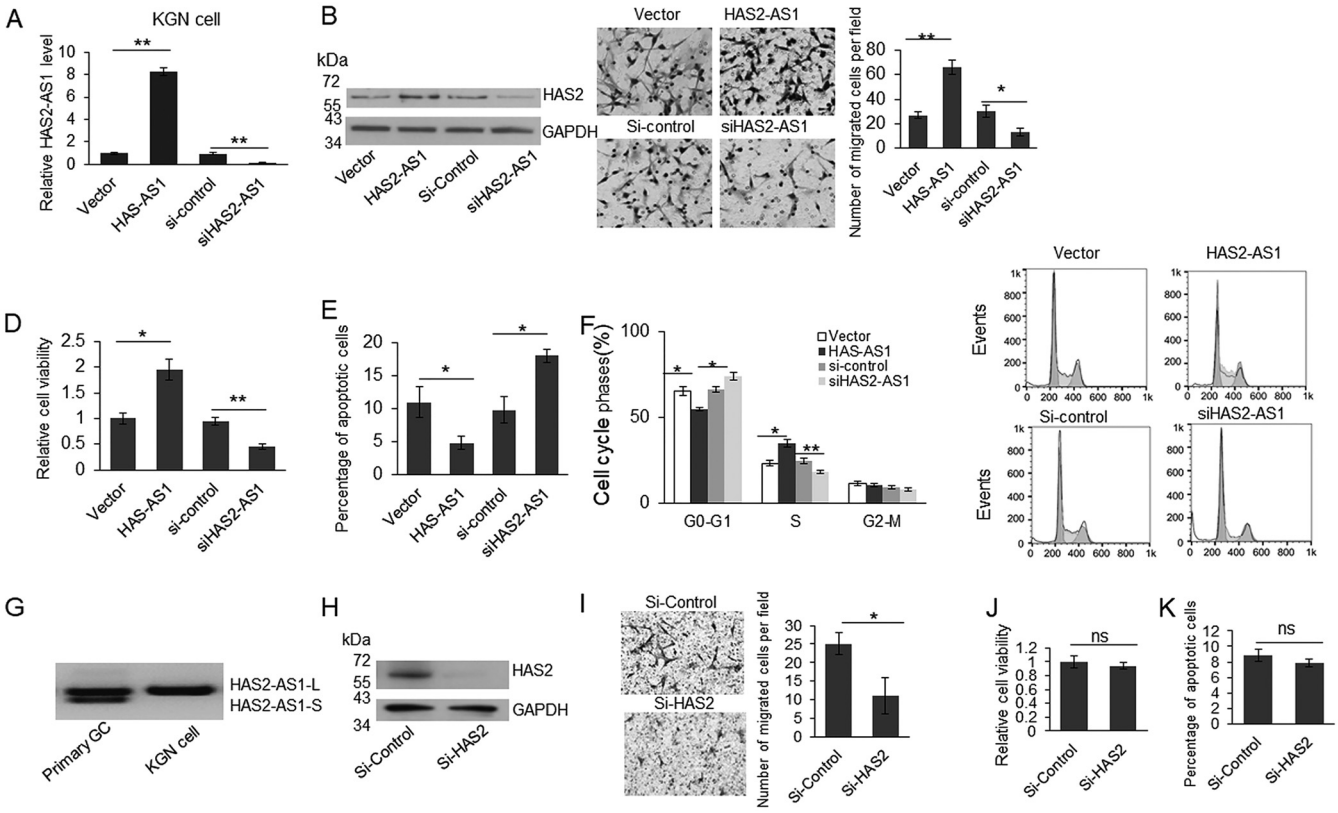

FIG 2 HAS2-AS1 promotes migration and proliferation and inhibits apoptosis in GCs. (A to F) KGN cells were transfected with a HAS2-AS1 overexpression vector or siRNA for 48 h, and then the cells were subjected to RT-qPCR (A), immunoblotting (B), transwell assay (C), MTT assay (D), and flow cytometry analysis (E and F). (G to J) KGN cells were transfected with siHAS2 or control siRNA for 48 h, and then the cells were subjected to immunoblotting (G), transwell assay (H), MTT assay (I), and flow cytometry analysis (J). Results were analyzed by paired Student's *t* test, and a *P* value of <0.05 was considered significant. *, $P < 0.05$; **, $P < 0.01$.

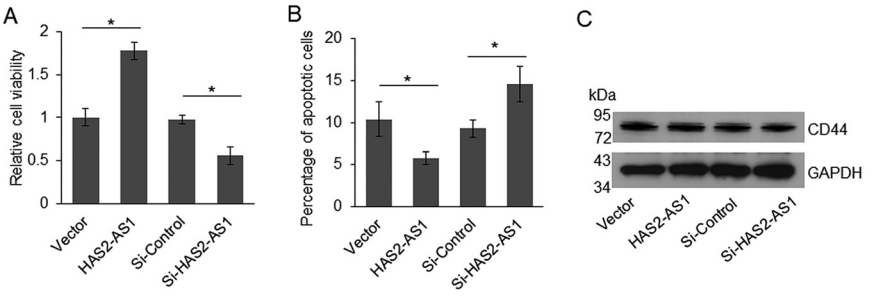

FIG 3 HAS2-AS1 regulates proliferation and apoptosis in a HA/HA receptor-independent manner. KGN cells were transfected with HAS2-AS1 expression vector or siHAS2 and then cultured in medium containing hyaluronic acid (HA) (molecular weight 5 kDa, 100 nM) for 48 h. The cells were then subjected to MTT assay (A), flow cytometry analysis (B), and immunoblotting (C).

GC migration, proliferation, and apoptosis, KGN cells were subjected to a transwell assay, 3-(4,5-dimethylthiazol-2-yl)-5-(3-carboxymethoxyphenyl)-2-(4-sulfophenyl)-2H-tetrazolium (MTT) assay, and flow cytometry to examine the cell migration capacity, cell viability, apoptosis, and cell cycle. As shown in Fig. 2C to E, HAS2-AS1-overexpressing cells had increased migration, upregulated viability, and reduced apoptosis. In contrast, HAS2-AS1 knockdown cells had reduced migration, inhibited cell viability, and increased apoptosis. Meanwhile, more HAS2-AS1-overexpressing KGN cells were distributed in the S phase, while more HAS2-AS1 knockdown cells were distributed in the G_0-G_1 phase (Fig. 2F).

Through Northern blotting, we determined that the longer isoform of HAS2-AS1 (HAS2-AS1-L) was the main isoform expressed in primary GCs and KGN cells (Fig. 2G). To understand the function of these two HAS2-AS1 isoforms, KGN cells were transfected with one isoform of HAS2-AS1. We noticed that both HAS2-AS1 isoforms upregulated migration and proliferation and inhibited apoptosis in KGN cells (data not shown). However, no significant difference was found between the HAS2-AS1-L and short (HAS-AS1-S) groups (data not shown). So, the subsequent research focused on the HAS2-AS1 longer isoform.

To identify whether HAS2-AS1 promoted cell migration proliferation and inhibited apoptosis through upregulating HAS2, KGN cells were transfected with HAS2-specific siRNA to knock down the endogenous HAS2 protein level, and then the cells were subjected to a transwell assay, MTT assay, and flow cytometry. As shown in Fig. 2H, the HAS2 protein level was significantly reduced by siHAS2. siHAS2 significantly repressed the number of migrated cells (Fig. 2I). However, siHAS2 did not restore the function of HAS2-AS1 in terms of cell viability and apoptosis (Fig. 2J and K), suggesting that HAS2-AS1 promotes cell proliferation and inhibits apoptosis through a HAS2-independent manner.

To examine whether HAS2-AS1-related cell proliferation and apoptosis occurs through an HA-related signaling pathway, HAS2-AS1-overexpressing or knockdown KGN cells were cultured in medium containing HA for 48 h. As shown in Fig. 3, HAS2-AS1 promoted KGN cell proliferation and inhibited apoptosis without changing the CD44 protein level, indicating that HAS2-AS1 regulated cell proliferation and apoptosis via an HA- and HA receptor-independent pathway.

HAS2-AS1 repressed TGF-β signaling by inhibiting TGFBR2 expression. To understand the mechanisms of how HAS2-AS1 controls proliferation and apoptosis in granulosa cells, HAS2-AS1 was transiently overexpressed or knocked down in KGN cells. Key components in the Akt, NF-κB, and TGF-β signaling pathways were examined by using immunoblotting. We observed that the levels of phosphorated PI3K and Akt were not significantly altered (data not shown). Meanwhile, in lipopolysaccharide-treated KGN cells, the levels of phosphorylated NF-κB and IκBα were not significantly changed (data not shown), indicating that HAS2-AS1 is not involved in the Akt and NF-κB signaling pathway. We noticed that the TGF-β receptor type 2 (TGFBR2) level was repressed by HAS2-AS1 and upregulated by HAS2-AS1 siRNA (Fig. 4A). Additionally, the HAS2-AS1 level was significantly upregulated from 2 to 48 h after TGF-β treatment (Fig. 4B), suggesting some interactions between TGF-β signaling and HAS2-AS1 in GCs.

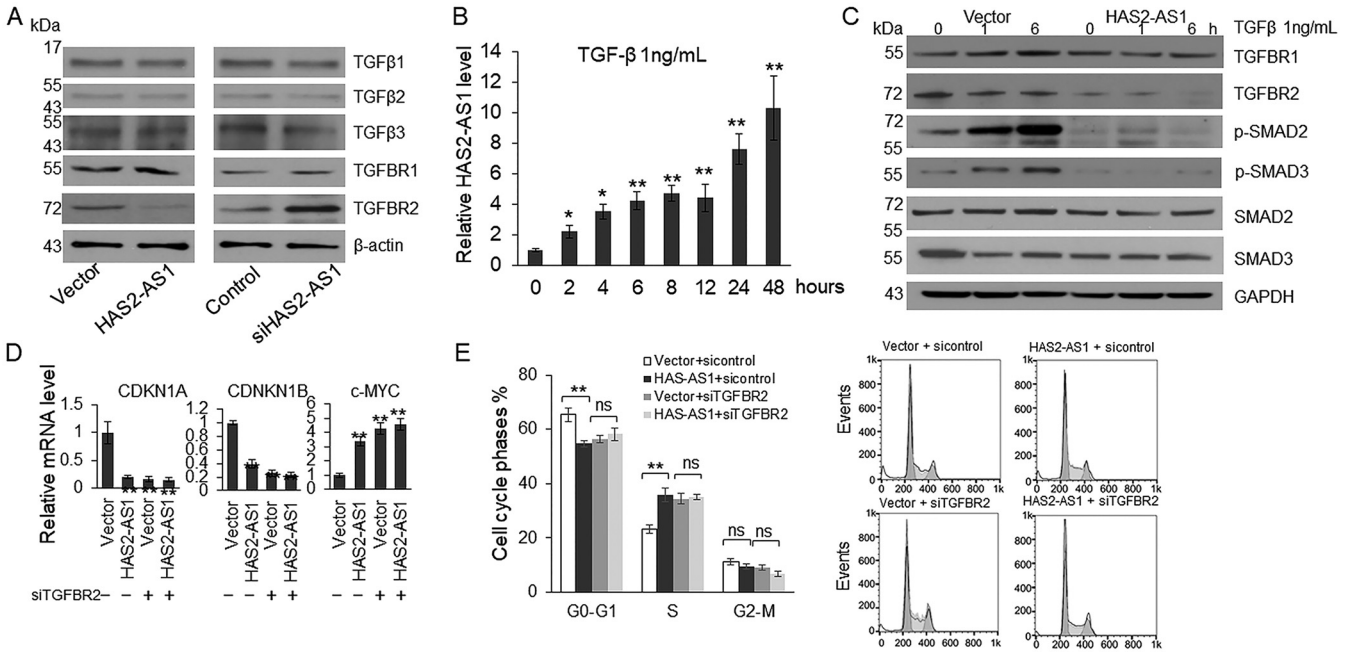

FIG 4 HAS2-AS1 inhibits TGF-β signaling by repressing TGFBR2. (A) KGN cells were treated with 1 ng/mL TGF-β. The relative HAS2-AS1 level was quantified by RT-qPCR at different time points. (B) KGN cells were transfected with HAS2-AS1 overexpression vector or siHAS-AS1 for 48 h. The expression levels of TGF-β1, TGF-β2, TGF-β3, TGFBR1, and TGFBR2 was examined by immunoblotting, with the level of GAPDH as a loading control. (C) Control and HAS2-AS1-overexpressing KGN cells were treated with 1 ng/mL TGF-β1 for 1 h or 6 h. The levels of TGFBR1, TGFBR2, SMAD2, SMAD3, p-SMAD2, and p-SMAD3 were examined by immunoblotting, with the level of GAPDH as a loading control. (D) The mRNA level of CDKN1A, CDKN1B, and c-MYC were examined by RT-qPCR. (E) The HAS2-AS1 overexpression vector and siTGFBR2 were cotransfected into KGN cells for 48 h, and then the cells were subjected to flow cytometry analysis. Results were analyzed by one-way ANOVA, and a P value of <0.05 was considered significant. *, $P < 0.05$; **, $P < 0.01$.

To understand whether HAS2-AS1 inhibits TGF-β signaling through repressing TGFBR2 expression, HAS2-AS1-overexpressing and wild-type KGN cells were treated with TGF-β for up to 6 h and then the cells were subjected to immunoblotting. As shown in Fig. 4C, the levels of phosphorylated SMAD2 and SMAD3 were increased in wild-type cells at 1 h and 6 h after treatment. However, no significant upregulation of p-SMAD2 and p-SMAD3 was observed in HAS2-AS1-overexpressing cells. Meanwhile, significantly reduced CDKN1A and CDKN1B and upregulated c-MYC were found in HAS2-AS1-overexpressing cells (Fig. 4D). When we examined the cell cycle by using flow cytometry, we found that 12% more HAS2-AS1-overexpressing cells switched from G_0/G_1 phase to S phase compared with control cells (Fig. 4E). When TGFBR2 was knocked down, the cell cycle distribution was similar in HAS2-AS1-overexpressing and control cells.

HAS2-AS1 regulates TGFBR2 promoter region hypermethylation by binding with EZH2. It has been reported that lysine 27 on histone 3 (H3K27) in the promoter region of TGFBR2 can be methylated by EZH2, which is related to TGFBR2 expression repression (25, 26). In addition, several lncRNAs have been reported to bind with EZH2 and contribute to the hypermethylation of target gene promoter regions. So, we hypothesized that HAS2-AS1 regulates TGFBR2 through binding with EZH2, which further induces hypermethylation of the TGFBR2 promoter region.

To confirm this hypothesis, endogenous EZH2 in KGN cells was knocked down by EZH2-specific siRNAs, and then the expression of TGFBR2 was detected by immunoblotting. As shown in Fig. 5A, the total H3K27me3 level was reduced in EZH2 knockdown cells and in cells treated with the EZH2 inhibitor 3-deazaneplanocin A (DZNep). Meanwhile, the level of TGFBR2 was increased, indicating that EZH2 regulates TGFBR2 expression through inducing hypermethylation. To understand whether HAS2-AS1 regulates TGFBR2 expression through regulating the hypermethylation of the promoter region, the H3K27me3 level was detected in HAS2-AS1-overexpressing and knockdown cells. As shown in Fig. 5B, HAS2-AS1 overexpression upregulated the H3K27me3 level while HAS2-AS1 knockdown reduced the

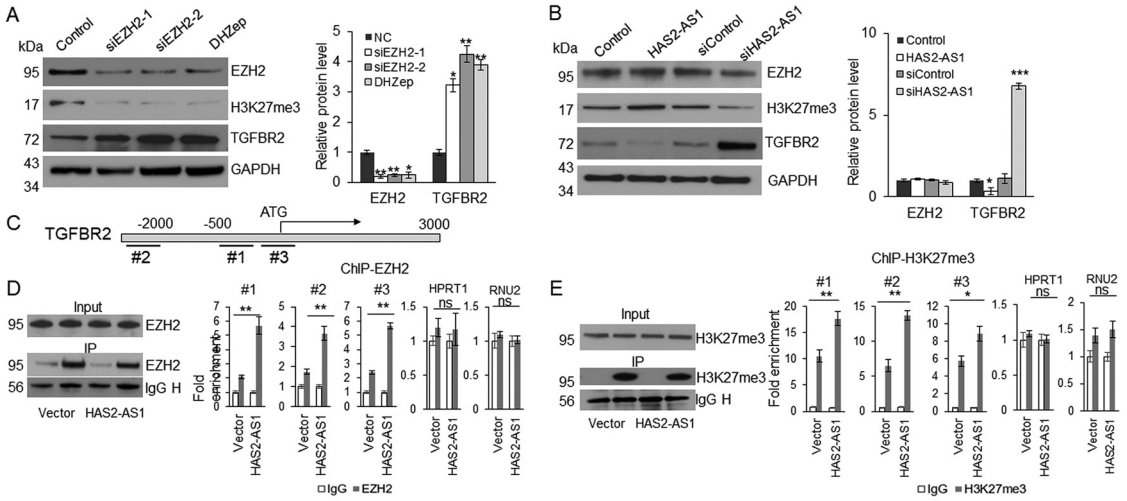

FIG 5 HAS2-AS1 regulates TGFBR2 expression through modulating promoter region hypermethylation. (A) KGN cells were transfected with EZH2-specific siRNAs or treated with DHZep for 48 h, and then the cells were subjected to immunoblotting. The relative gene expression levels were quantified with ImageJ, and the results were analyzed by a one-way ANOVA. (B) Immunoblotting to examine the EZH2, H3K27me3, and TGFBR2 levels in HAS2-AS1 overexpression or knockdown KGN cells. The relative gene expression levels were quantified with ImageJ, and the results were analyzed with a one-way ANOVA. (C) Schematic diagram of the TGFBR2 promoter region and primer design. (D) ChIP assay with EZH2 antibody. The enrichment of EZH2 was confirmed by immunoblotting, and the enrichment of the TGFBR2 promoter region was examined by RT-qPCR. (E) ChIP assay with H3K27me3 antibody. The enrichment of EZH2 was confirmed by immunoblotting, and the enrichment of the TGFBR2 promoter region was examined by RT-qPCR. Results were analyzed by Student's *t* test, and a *P* value of <0.05 was considered significant. *, $P < 0.05$; **, $P < 0.01$.

H3K27me3 level without changing the EZH2 protein level, suggesting that HAS2-AS1 may function as a cofactor of EZH2, guiding EZH2 to methylate the promoter regions of target genes.

To identify whether HAS2-AS1 regulates the binding of EZH2 to the TGFBR2 promoter region and induces H3 hypermethylation, a chromatin immunoprecipitation-PCR (ChIP-PCR) assay was used to determine how much DNA in the TGFBR2 promoter region (Fig. 5C) was bound by EZH2 and hypermethylated H3. As shown in Fig. 5D, EZH2 was successfully enriched by EZH2 antibody in both control and HAS2-AS1-overexpressing KGN cells. Three segments of the TGFBR2 promoter region were enriched by EZH2 antibody in both control and HAS2-AS1-overexpressing cells, indicating that EZH2 binds to the TGFBR2 promoter region. Furthermore, EZH2 antibody enriched more TGFBR2 promoter segments in HAS2-AS1-overexpressing cells, indicating that EZH2 functions as a cofactor guiding EZH2 to the promoter region of TGFBR2. Similarly, H3K27me3 was successfully enriched by H3K27me3 antibody compared with mouse IgG (Fig. 5E). Three segments of the TGFBR2 promoter region were enriched by H3K27me3 antibody in both control and HAS2-AS1-overexpressing cells. Meanwhile, H3K27me3 antibody enriched more TGFBR2 promoter segments in HAS2-AS1-overexpressing cells, indicating that HAS2-AS1 upregulated the hypermethylation level of the TGFBR2 promoter region (Fig. 5E).

To confirm the interaction between HAS2-AS1 and EZH2 and identify the EZH2-binding sites on HAS2-AS1, four overlapping segments of HAS2-AS1 were transcribed *in vitro* for an RNA pulldown assay (Fig. 6A). We observed that only segment 1 could successfully recruit EZH2 from the cell lysate (Fig. 6B). It has been reported that EZH2 preferably binds to G-quadruplex RNA sequences (27). So, we predicted the G-quadruplex domains in the first segment of HAS2-AS1 by using the G4RNA screener web server (https://bioinformatics.ramapo.edu/QGRS/index.php) (28) and then constructed a plasmid expressing a truncated form of HAS2-AS1, without the 142-bp sequence containing the first two G-quadruplex domains that had the highest G-score (Fig. 6C and D). Through the RNA pulldown assay, we confirmed that the truncated HAS2-AS1 could not bind with EZH2 (Fig. 6E), indicating that EZH2 binds with this 142-bp segment of HAS2-AS1. To investigate whether HAS2-AS1 modulates proliferation, apoptosis, and the cell cycle of granulosa cells via the interaction of HAS2-AS1 and EZH2, HAS2-AS1Δ was overexpressed in wild-type or HAS2-AS1wt knockdown

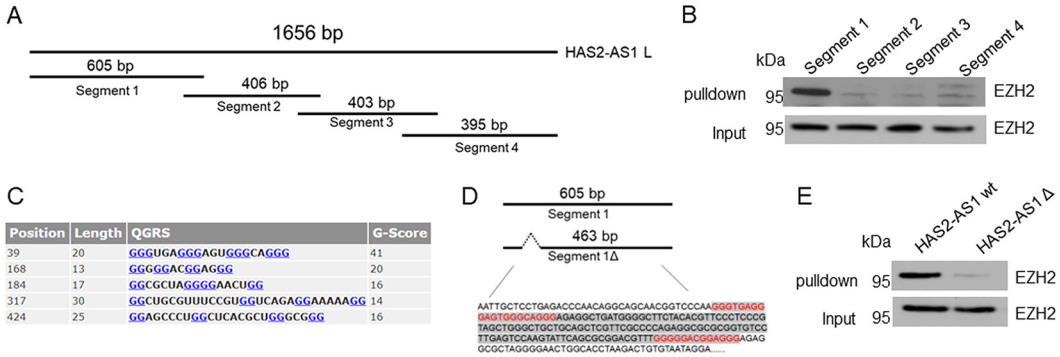

FIG 6 EZH2 binds with G-quadruplex domains of HAS2-AS1. (A) Schematic diagram of four overlapping segments of the HAS2-AS1 longer isoform. (B) RNA pulldown assay with four segments of HAS2-AS1. (C) Predicted G-quadruplex domains in the first segment of HAS2-AS1. (D) Schematic diagram of truncated HAS2-AS1 first segment construction. Red letters indicate G-quadruplex domains. Deleted nucleotides are labeled with gray shade. (E) RNA pulldown assay with wild-type HAS2-AS1 or HAS2-AS1 with the binding region deleted.

KGN cells (Fig. 7A). As shown in Fig. 7B, HAS2-AS1Δ did not repress TGFBR2 expression, and HAS2-AS1Δ overexpression could not rescue the repressive effect of siHAS2-AS1wt on TGFBR2 expression. Meanwhile, HAS2-AS1Δ-overexpressing KGN cells had similar viability, apoptotic cell proportions, downstream gene expression levels, and cell cycles as the controls, and HAS2-AS1Δ could not rescue the phenotypes of siHAS2-AS1wt-treated cells (Fig. 7C to F). These results indicate that the binding of HAS2-AS1 and EZH2 is necessary for the function of HAS2-AS1 in regulating cell viability, apoptosis, and the cell cycle.

HAS2-AS1 binds with EZH2 and colocalizes with EZH2 in the cell nucleus. To further confirm that EZH2 can bind with HAS2-AS1 in granulosa cells, the cell nucleus and cytoplasm were separated from KGN cells, and these cell fractions were subjected to RNA extraction, RT-qPCR, and immunoblotting. As shown in Fig. 8A, the cell nucleus-localized RNA MALAT1 was specifically detected in the nucleus fraction, and the cytoplasm-localized RNA

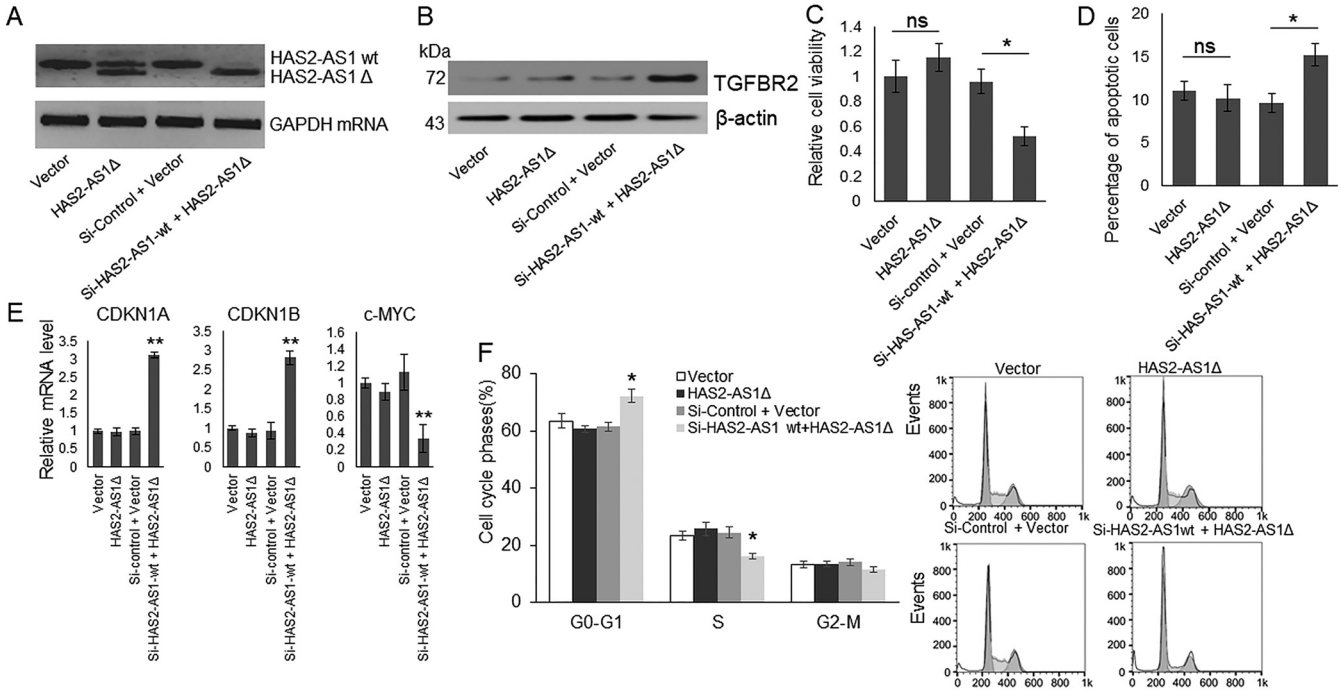

FIG 7 Binding with EZH2 is necessary for HAS2-AS1 function in regulating TGFBR2 expression, cell viability, apoptosis, and the cell cycle. HAS2-AS1Δ was overexpressed in wild type or HAS2-AS1wt knockdown KGN cells. (A) Expression of HAS2-AS1Δ and HAS2-AS1wt was detected by Northern blotting. (B) The protein level of TGFBR2 was determined by immunoblotting. (C and D) Cell viability was detected by MTT assay, and apoptotic cells were examined by flow cytometry analysis (D). (E and F) The expression levels of CDKN1A, CDKN1B, and c-MYC were detected by RT-qPCR (E), and the cell cycle was examined by flow cytometry (F). Results were analyzed by a one-way ANOVA, and *P* values of <0.05 were considered significant. *, $P < 0.05$; **, $P < 0.01$.

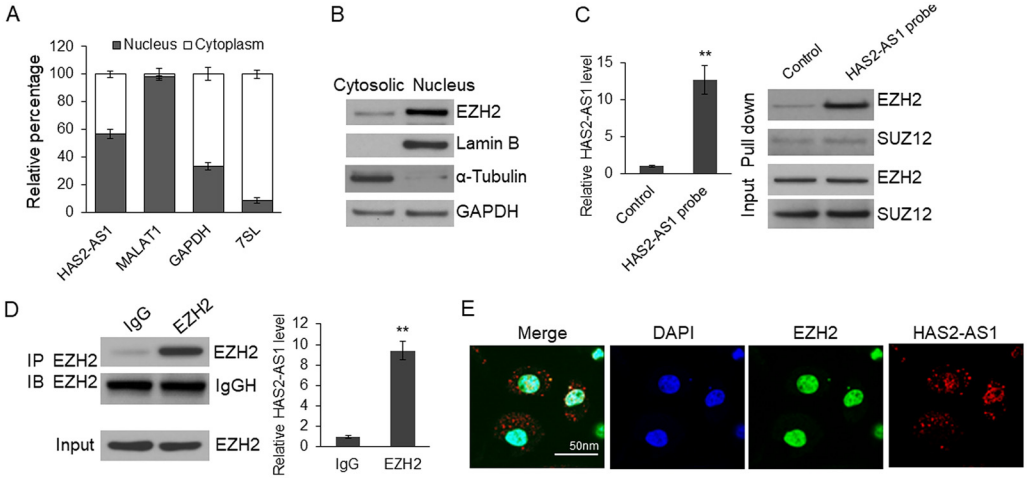

FIG 8 HAS2-AS1 binds with EZH2 and colocalizes with EZH2 in the cell nucleus. (A) RNA was isolated from the whole KGN cells or from cytoplasm and nucleus separately. The relative levels of HAS2-AS1, MALAT1, and GAPDH were determined by RT-qPCR. (B) The nuclear and cytosol fractions were isolated from KGN cells, and then the EZH2 level was detected by immunoblotting. (C) RAP assay. Biotin-labeled HAS2-AS1-specific DNA probe was incubated with KGN cell lysate to recruit endogenous HAS2-AS1. The HAS2-AS1 was precipitated by streptavidin beads. The enrichment of HAS2-AS1 was confirmed by RT-qPCR, and the HAS2-AS1 binding proteins were subjected to immunoblotting. (D) RIP assay. EZH2- and EZH2-binding RNAs were recruited by antibody-coated beads and then subjected to immunoblotting and RT-qPCR. (E) The colocalization between endogenous HAS2-AS1 and EZH2 was examined by *in situ* hybridization combined with immunofluorescence. Results were analyzed by Student's *t* test, and a *P* value of <0.05 was considered significant. *, $P < 0.05$; **, $P < 0.01$.

7SL was mainly detected in the cytoplasmic fraction, which confirmed the fractionation quality. HAS2-AS1 was detected in both cytosol and nucleus, like glyceraldehyde-3-phosphate dehydrogenase (GAPDH), indicating that HAS2-AS1 was distributed in both the cell nucleus and cytoplasm. Similarly, Lamin B protein was mainly observed in the nucleus, while α-tubulin was mainly found in the cytosol, indicating that cell fraction isolation was successful (Fig. 8B). EZH2 was observed mainly in the nucleus (Fig. 8B), providing a spatial colocalization potential of HAS2-AS1 and EZH2. Subsequent results in an RNA antisense purification (RAP) assay with cell nucleus extracts showed that HAS2-AS1 was enriched more than 12-fold by the HAS2-AS1-specific probe (Fig. 8C). EZH2 and not SUZ12 was enriched by the HAS2-AS1 probe at the same time, suggesting that HAS2-AS1 may bind with EZH2 in the cell nucleus (Fig. 8C). In contrast, an RNA immunoprecipitation-PCR assay was used to confirm binding between HAS2-AS1 and EZH2. As shown in Fig. 8D, EZH2 was enriched by EZH2 antibody. Meanwhile, HAS-AS1 was recruited by EZH2 antibody, indicating that EZH2 can bind with HAS2-AS1 in KGN cells. Finally, the localizations of EZH2 and HAS2-AS1 in KGN cells were examined by immunofluorescence. As shown in Fig. 8E, EZH2 and HAS2-AS1 colocalized in the cell nucleus.

HAS2-AS1 regulates TGFBR2 expression in primary GCs by modulating H3K27me3 in the promoter region. To further confirm our findings in primary GCs, we isolated and cultured primary GCs from 5 patients with PCOS and 5 healthy controls. We examined the expression of HAS2-AS1, HAS2, TGFBR2, and H3K27m3 in the TGFBR2 promoter region. The results indicated that the levels of HAS2-AS1 and HAS2 were both increased in GCs from patients with PCOS (Fig. 9A and B), and the TGFBR2 level was downregulated (Fig. 9B). The H3K27me3 level was increased in the promoter region of TGFBR2 (Fig. 9C and D), which may have been a result of increased colocalization of HAS2-AS1 and EZH2 (Fig. 9E). Knockdown HAS2-AS1 repressed HAS2 expression and increased the TGFBR2 level in the primary GCs (Fig. 9F and G). Primary GCs from patients with PCOS exhibited increased S-phase cell numbers (Fig. 9H), migration capacity (Fig. 9I), and viability (Fig. 9J) and repressed apoptosis (Fig. 9K).

DISCUSSION

HAS2-AS1 has been found to regulate the HAS2 protein level, but the processes can be in totally different manners in different cell types. In the normal reproduction system, the level of HAS2-AS1 is very low in immature GCs but is increased in mature GCs (14). However, the

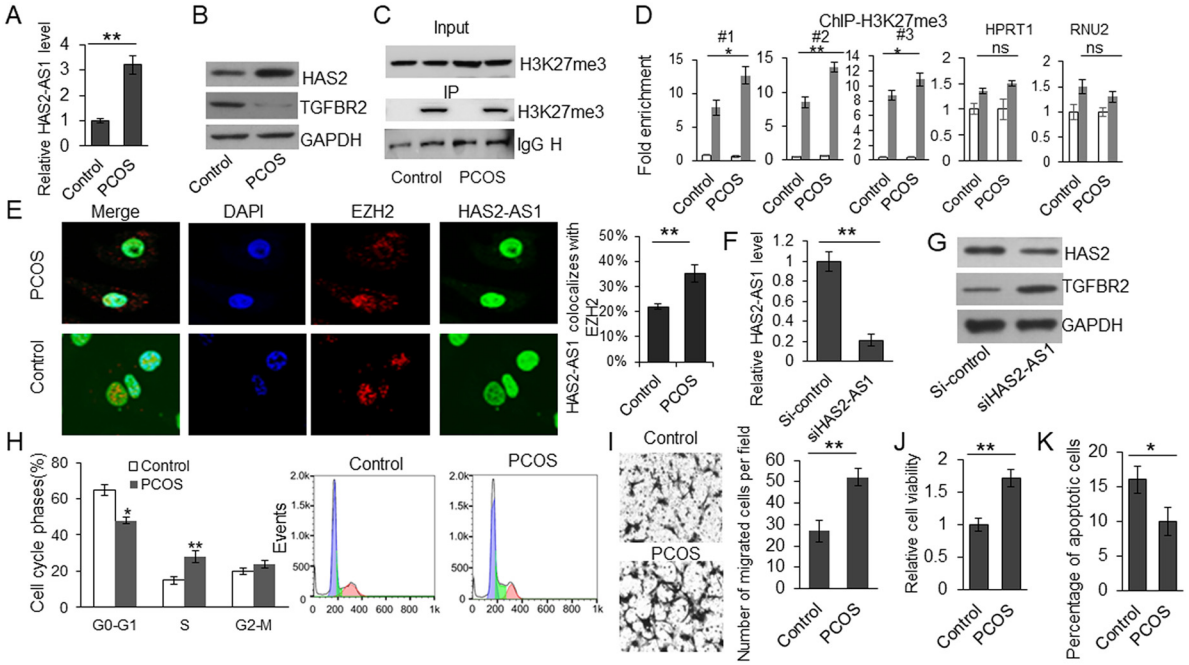

FIG 9 HAS2-AS1 regulates TGFBR2 expression in primary GCs. (A to E) Primary GCs from 5 controls and 5 patients with PCOS were cultured *in vitro* and then subjected to RT-qPCR (A), immunoblotting (B), ChIP assay (C and D), and immunofluorescence (E). (F and G) Primary GCs from patients with PCOS were transfected with siHAS2-AS1 for 48 h and then subjected to RT-qPCR (F) and immunoblotting (G). (H to K) Primary GCs from 5 controls and 5 patients with PCOS were cultured *in vitro* and then subjected to flow cytometry for cell cycle analysis (H), migration assay (I), MTT assay (J), and flow cytometry for apoptosis analysis (K). Results were analyzed by Student's *t* test, and *P* values of <0.05 were considered significant. *, $P < 0.05$; **, $P < 0.01$.

function of HAS2-AS1 in the pathophysiological processes of PCOS is totally unknown. In the present study, we identified that HAS2-AS1 is overexpressed in patients with PCOS and positively regulated by HAS2 protein levels in GCs. To our understanding, this is the first report demonstrating the roles of HAS2-AS1 in PCOS, which unveiled the regulatory relations between HAS2-AS1 and HAS2 in GCs.

Emerging evidence indicates that the TGF-β signaling pathway plays critical roles in maintaining the normal physiological conditions of the placenta, while dysregulated TGF-β signaling has been found disordered in patients with PCOS. For example, genetic studies have constructed the linkage between PCOS and a polymorphism in intron 55 of the fibrillin 3 gene, which was considered to bind with and inactivate TGF-βs (29, 30). Meanwhile, upregulated follistatin and downregulated activin in serum has been observed in patients with PCOS (16, 17). Our previous study also confirmed that the TGF-β signaling pathway was repressed in the GCs from patients with PCOS (31). In the present study, we confirmed that HAS2-AS1 upregulation is related to GC dysfunction through repressing TGF-β signaling, and this successfully constructed the correlation between the disordered HAS2–AS1–TGF-β axis and the etiology of PCOS.

The phenomenon of inhibition of HAS2-AS1 results in HAS2 expression reduction and decreases migration of granulosa cells as reported by Yuval Yung and colleagues in 2019 (14). Our research confirmed these findings in KGN cells. Furthermore, we identified that HAS2-AS1 regulates GC proliferation, apoptosis, and cell cycle distributions through a HAS2-independent pathway. Most recently, the HAS2-independent functions of HAS2-AS1 were observed by Arianna Parnigoni and colleagues in breast cancer cells (32). They confirmed in estrogen receptor-negative breast cancer cells that HAS2-AS1 inhibits breast cancer cell aggressiveness via modulating several signaling pathways, such as TGF-β and PI3K-Akt (32). TGF-β has been found to regulate HAS2-AS1 expression in proximal tubule cell (PTC), but whether HAS2-AS1 regulates TGF-β signaling as a feedback mechanism is unknown. In the present study, we identified for the first time that HAS2-AS1 functioned as a TGF-β signaling repressor by regulating the hypermethylation of the TGFBR2 promoter region. We determined that upregulated

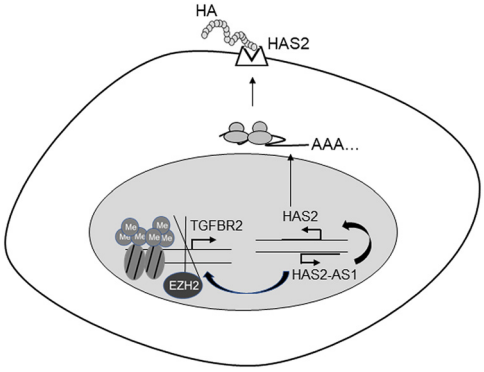

FIG 10 Schematic diagram of HAS2-AS1 function in GCs.

HAS2-AS1 repressed TGFBR2 expression through enhancing the hypermethylation level of the promoter region, which functioned like a negative feedback mechanism.

It has been found that HAS2-AS1 can promote histone O-GlcNAcylation and increase the accessibility index of the proximal promoters of both HAS2 and HAS2-AS1, indicating that HAS2-AS1 has the potential to regulate multiple gene expression via modulating chromatin structure (13). EZH2 and SUZ12 are two key components of polycomb repressive complex 2 (PRC2) that have been determined to have RNA-binding motifs (33). Meanwhile, some lncRNAs have been reported to recruit PRC2 to specific sites for epigenetic repression via binding with EZH2 or SUZ12 (34–36). In the present study, we identified for the first time that HAS2-AS1 colocalizes with EZH2 in the nucleus and interacts with EZH2 not SUZ12 in GCs, which further induces promoter region hypermethylation of TGFBR2 (Fig. 10). These findings expand our knowledge of HAS2-AS1.

There are still limits of this research: (i) The underlying mechanism of how HAS2-AS1 guides PRC2 to the TGFBR2 promoter region needs to be further unveiled. (ii) HAS2-AS1 may guide PRC2 to several target sites in the genome and not only TGFBR2. All target sites of HAS2-AS1 need to be identified by high-throughput methods.

In conclusion, this study determined that HAS2-AS1 overexpression contributes to GC dysfunction by regulating HAS2 expression and TGF-β signaling, which partially unveiled the mechanism of the pathophysiological processes of PCOS.

MATERIALS AND METHODS

Participants. Seventy-six patients with PCOS and 18 healthy women were recruited at The Second Affiliated Hospital of Zhengzhou University. They were diagnosed to have healthy ovaries and did not have male

TABLE 1 Basic clinical features of participants

Clinical feature[a]	Controls (n = 18)	PCOS[b] (n = 76)
Age (yrs)	29.63 ± 6.42	28.44 ± 2.93
BMI (kg/m^2)	22.42 ± 4.66	24.45 ± 5.73
Total T (nmol/liter)	1.33 ± 0.41	2.88 ± 0.92*
Free T (pmol/liter)	19.07 ± 5.12	42.33 ± 9.43**
E2 (nmol/liter)	0.22 ± 0.115	0.23 ± 0.164
SHBG (nmol/liter)	52.41 ± 6.23	50.12 ± 8.16
DHEAS (μmol/liter)	4.52 ± 0.65	5.47 ± 1.08
FSH (IU/liter)	6.02 ± 1.12	6.01 ± 1.67
LH (IU/liter)	5.86 ± 1.71	6.18 ± 1.87
Prolactin (ng/mL)	13.02 ± 1.32	12.47 ± 1.93
Fasting insulin (mIU/mL)	8.74 ± 3.17	11.83 ± 5.54*
Fasting glucose (mmol/liter)	5.45 ± 0.75	6.08 ± 1.13
Menstrual cycle (days)	29.13 ± 5.54	44.22 ± 9.64*
Normal menstrual cycle	18/18	33/76

[a]T, testosterone; E2, estradiol; SHBG, sex hormone-binding globulin; DHEAS, dehydroepiandrosterone-sulfate; FSH, follicle stimulating hormone; LH, luteinizing hormone.
[b]Values for PCOS subjects were significantly different: *, $P < 0.05$; **, $P < 0.01$.

factor infertility. Written informed consent was obtained from all participants and this study was approved by the Ethics Committee of The Second Affiliated Hospital of Zhengzhou University. The revised diagnostic criteria of the 2003 Rotterdam meeting (37) were used to identify the PCOS phenotypes, which necessitated the inclusion of at least two of the following criteria: (i) signs of clinical and/or biochemical hyperandrogenism, (ii) oligo and/or anovulation, and (iii) polycystic ovaries. Healthy women ($n = 18$) with normal menstruation were recruited as controls. The clinical characteristics of all participants are shown in Table 1.

Clinical and biochemical measurements. A physical examination was performed, including weight, height, and body mass index (BMI, in kilograms per square meter). After 10 h of fasting, blood samples were collected, and the serum samples were separated by centrifugation and stored at −20°C prior to analysis. The serum hormone levels, including follicle-stimulating hormone (FSH), sex hormone-binding globulin (SHBG), estradiol (E2), luteinizing hormone (LH), testosterone (T), dehydroepiandrosterone-sulfate (DHEAS), prolactin, and insulin, were measured using enzyme-linked immunosorbent assay kits (Abcam, Cambridge, MA, USA).

Follicular fluid and granulosa cell collection. Human granulosa cells were obtained from follicles (diameters of >12 mm) from all participants. Follicular fluid of 2 follicles from the same participant was collected for granulosa cell isolation. After filtration using a 40-μm cell strainer (Fisher Scientific, Pittsburgh, PA, USA), the blood cells were excluded after sorting using CD45 microbeads (Miltenyi Biotec, Bergisch Gladbach, NRW, Germany). The cells were collected after centrifugation and stored at −80°C for further experiments. Primary GCs separated from 5 healthy controls were cultured for functional study.

Cell culture and treatment. Human granulosa-like tumor cell line KGN and primary granulosa cells were maintained in Dulbecco's modified Eagle medium (DMEM)-F12 containing 10% fetal bovine serum (HyClone), 100 IU/mL penicillin, and 100 IU/mL streptomycin (HyClone). All cells were maintained at 37°C under an atmosphere of 5% CO_2.

To examine whether HAS2-AS1 expression is regulated by TGF-β, 1 ng/mL TGF-β1 (Thermo Fisher Scientific) was added to the cell culture medium directly, and then the cells were collected at 0, 2, 4, 6, 8, 12, 24, and 48 h. The cells were then subjected to RNA extraction, and the HAS2-AS1 levels were examined by RT-qPCR.

Vector construction. The full lengths of HAS2-AS1-L and HAS2-AS1-S were amplified by RT-PCR and then cloned into a pcDNA3.1 vector between the NheI and ApaI sites, respectively. Primers were the following: HAS2-AS1-NheF, CTAGCTAGCAATTGCTCCTGAGACCCAACAGG; HAS2-AS1-ApaR, GCGGGCCCGCATTTATTATTAC TTCAAATGACTTAA.

Cell transfection. The cells were seeded at a density of 2×10^5/mL, and the medium was then replaced with fresh DMEM-F12 without antibiotics.

The vectors were transfected into KGN cells and primary GCs by using an electroporator (Lonza) with a P1 Primary Cell 4D-nucleofector X kit. siRNAs (50 nM) were transfected into KGN cells and primary GCs by using Lipofectamine 2000 (Thermo Fisher Scientific) following the manufacturer's instructions. At 48 h post-transfection, the cells were harvested by mild trypsinization and washed in phosphate-buffered saline.

The siRNA sequences were the following: SiHAS2-AS1, GGAACUGCCGUGACGAAUUTT; SiHAS2, GGAAGAUUG GUACAAUCAAGAAUTT; SiTGFBR2, GAACUGAUGCUUCCUGGAAAACCAA; Sicontrol, CACCUCUAGUUGUCCCUGATT.

***In vitro* transcription.** The full-length HAS2-AS1, with EZH2 binding sites deleted, HAS2-AS1(HAS2-AS1Δ), and four segments of HAS2-AS1 were amplified by RT-PCR with forward primers containing T7 promoter sequence (TAATACGACTCACTATAGGG) and then purified after electrophoresis. Biotin-labeled RNAs were obtained by using T7 RiboMAX Express large-scale RNA production system (Promega) with biotin-16-UTP (Sigma). The RNA concentration and purity were determined using a model ND-2000 spectrophotometer (Nanodrop Technologies, Wilmington, DE, USA).

RNA pulldown. For RNA pulldown assay, 1 mg of protein extract was diluted with NT2 buffer (50 mM Tris-HCl [pH 7.4], 150 mM NaCl, 1 mM $MgCl_2$, 0.05% NP-40 supplemented with fresh RNaseOut [200 U], 400 μM ribonucleoside vanadyl complex (RVC), 1 mM dithiothreitol [DTT], 20 mM EDTA, and protease inhibitor cocktail) and then incubated with 50 pmol biotin-labeled RNA at 4°C for 2 h. After 1 h of incubation with streptavidin beads, the RNA protein complexes were washed with NT2 buffer 6 times. The enriched proteins were then subjected to immunoblotting.

RNA extraction. TRIzol reagent (Invitrogen) was used to extract RNA from all the samples, according to the manufacturer's instructions. Briefly, samples were resuspended with 100 μL phosphate-buffered saline (PBS) and then mixed with 1 mL TRIzol. After mixing with 200 μL chloroform and centrifugation, the supernatants were transferred into a new tube and the RNAs were precipitated by isopropanol. The RNA pellets were washed by 70% ethanol and then resolved. The RNA concentration and purity were determined using a model ND-2000 spectrophotometer (Nanodrop Technologies, Wilmington, DE, USA). Only samples with absorbance ratios at 260 nm/280 nm of ~2.0 and at 260 nm/230 nm of 1.9 to 2.2 were considered for inclusion in the study.

Northern blotting. Five micrograms of total RNA was resolved on a 1% agarose–6.5% formaldehyde gel and electrophoretically transferred to nylon membranes (Sigma). After UV-cross-linking and baking at 80°C for 30 min, the membrane was prehybridized at 42°C for 4 h and then hybridized with digoxigenin-labeled HAS2-AS1-specific probe at 40°C overnight. After four washes, HAS2-AS1 was detected with an alkaline phosphatase-conjugated antidigoxigenin antibody (Sigma) with CDP-Star substrate (Thermo Fisher Scientific). The HAS2-AS1 probe had the following sequence: CTTGCAAGACCTGTGTCCTATTACACAGTCTTAGGTGCCAGTTCCC.

Quantitative RT-PCR. The HAS2-AS1 level was quantified by RT-PCR using SYBR green real-time PCR master mix (Thermo Fisher Scientific), with the GAPDH level as a loading control. Results were analyzed by Student's *t* test. Each sample in each group was measured in triplicate, and the experiment was repeated three times. Primer sequences were the following: HAS2-AS1-QF, GGTGTCCTTGAGTCCAAGTATT; HAS2-AS1-QR, TGCAAGACCTGTGTCCTATTAC; MALAT1-QF1, GCTCAGTTGCGTAATGGAAAG; MALAT1-QR1, GTGTTCTCTT GAGGGACAGTAG; GAPDH-QF, GGTGTGAACCATGAGAAGTATGA; GAPDH-QR, GAGTCCTTCCACGATACCAAAG; TGFBR2-promoter-1F, CAGCTGAAAGTCGGCCAAAG; TGFBR2-promoter-1R, AGCCCCTAGCTCTCTCGTAG; TG

FBR2-promoter-2F, GCAAGGAGAAGCCAAATGAAAG; TGFBR2-promoter-2R, CTTCCCACTGCTCTTGAGATAAA; TGFBR2-promoter-3F, CTCGGTCTATGACGAGCAG; TGFBR2-promoter-3R, ACTCACCCGACTTCTGAAC; HPRT1-QF, TGTTTGGGCTATTTACTAGTTG; HPRT1-QR, ATAAAATGACTTAAGCCCAGAG; 7SL-QF, GCACTAAGTTCGGCA TCAATATG; 7SL-QR, AGTGCAGTGGCTATTCACAG.

Immunoblotting. All protein samples were denatured by boiling in sodium dodecyl sulfate–β-mercaptoethanol loading buffer, and then 20-μg samples were separated using a 10% PAGE gel. The proteins in the gels were blotted onto a polyvinylidene fluoride membrane (Amersham Pharmacia Biotech, St. Albans, Herts, UK) by electrophoretic transfer and then incubated with one of the primary antibodies overnight at 4°C after blocking by 5% nonfat milk. The membranes were incubated with horseradish peroxidase-conjugated secondary antibody for another 2 h at room temperature, and then the signals were detected by using an ECL kit (Pierce, Appleton, WI, USA). The GAPDH signal was used as a loading control. Each sample was examined at least twice, and representative results are shown.

Transwell assay. A typical transwell assay (Costar; 6.5-mm diameter, 8-μm pore size) was used to examine the cell migration capacity. Briefly, 3×10^4 cells in 200 μL serum-free medium were seeded to the top chamber and 500 μL medium with 5% serum was added to the bottom. After 12 h, filters were then submerged in 4% paraformaldehyde for 15 min, and cells on the upper surface were removed with cotton swabs. The cells on the lower surface were stained with hematoxylin-eosin. Ten random fields were selected to determine the average number of cells per view field. The experiments were repeated independently at least three times, and representative results are shown.

RAP assay. Total cell extracts were incubated with a 57-bp biotin-labeled HAS2-AS1-specific probe, 5′-AACGGCGGGGAAGGAGAAGTCAAGACGTCTGGAAAGAATTACCCAGTCCTGGCTTCG-3′, or a sequence-scrambled probe, TCAACCTTTACACCGATCCTGGGTAATTCTTTCCAGACGTAGATTAGCCAGGTGCAA at 4°C for 4 h. The hybridized material was captured with magnetic streptavidin beads (Thermo Fisher Scientific). After six washes with wash buffer (50 mM Tris-HCl [pH 7.4], 150 mM NaCl, 1 mM $MgCl_2$, 0.05% NP-40 supplemented with fresh RNaseOut [200 U], 400 μM RVC, 1 mM DTT, 20 mM EDTA, and protease inhibitor cocktail), the proteins were boiled with loading buffer and the levels of EZH2 and SUZ12 were determined by immunoblotting. The experiments were repeated independently at least three times, and representative results are shown.

PAR-CLIP. For the photoactivatable ribonucleotide-enhanced cross-linking and immunoprecipitation (PAR-CLIP) assay, cells were seeded in 10-cm plates, and then 4-thiouridine was added to a final concentration of 100 μM, 12 h before cross-linking. The cells were washed with cold PBS 3 times and then irradiated uncovered with 0.15 J/cm^2 of 365-nm UV light. The cells were scraped off and lysed in lysis buffer (150 mM NaCl, 50 mM Tris-HCl [pH 7.5], 0.5% Triton X-100) on ice for 10 min. After 10 min of centrifugation at 13,000 $\times$ *g* at 4°C, the cell lysates were incubated with EZH2 antibody-coated magnetic beads for 4 h at 4°C. After incubation, the beads were washed 6 times with wash buffer (50 mM Tris-HCl [pH 7.4], 150 mM NaCl, 1 mM $MgCl_2$, 0.05% NP-40 supplemented with fresh RNaseOut [200 U], 400 μM RVC, 1 mM DTT, 20 mM EDTA, and protease inhibitor cocktail) and then subjected to immunoblotting and RNA extraction. The experiments were repeated independently at least three times, and representative results are shown.

Cytoplasm and nuclei fractionation. Cells were trypsinized and collected by centrifugation. After 3 washes, the cells were resuspended in cytoplasmic extract (CE) buffer (10 mM HEPES, 60 mM KCl, 1 mM EDTA, 0.075% NP40, 1 mM DTT; pH 7.6). The cells were incubated on ice for 3 min and then centrifuged at 250 $\times$ *g* for 5 min. The supernatant was removed to a new tube for RNA extraction, and the cell nuclei were washed four times with CE buffer without NP-40. After the final wash, the pellets were resuspended in 200 μL PBS and then subjected to RNA extraction. The experiments were repeated independently at least three times, and representative results are shown.

Chromatin immunoprecipitation assay. For the ChIP assay, KGN cells were cross-linked with 1% formaldehyde at 37°C for 5 min and then resuspended in SDS lysis buffer (1% SDS, 10 mM EDTA, 50 mM Tris-HCl; pH 8.1) for 15 min on ice. The cell lysates were sonicated on ice for 5 min. After centrifuging at 13,000 rpm at 4°C for 10 min, the supernatant was diluted 10 times in the dilution buffer (0.01% SDS, 1.1% Triton X-100, 1.2 mM EDTA, 167 mM NaCl, 16.7 mM Tris-HCl; pH 8.1) and was incubated for 1 h on a rotating platform at 4°C with protein A/G beads. The supernatant was incubated with specific antibody-coated beads for 6 h at 4°C, with rabbit IgG-coated beads as a negative control, and then the beads were washed with three times with LiCl buffer (0.25 M LiCl, 1% Triton X-100, 1% deoxycholic acid, 1 mM EDTA, 10 mM Tris-HCl; pH 8.1). After the final wash, half of the beads were subjected to immunoblotting and the other half were subjected to DNA extraction and qPCR. The experiments were repeated independently at least three times, and representative results are shown.

FISH and immunofluorescence. The HAS2-AS1 fluorescence *in situ* hybridization (FISH) and EZH2 immunofluorescence experiments were performed following the protocols reported by Hu Y et al. (38). Briefly, the cells were fixed with 4% formaldehyde at room temperature for 10 min and then permeabilized on ice for 10 min (PBS, 0.5% Triton X-100). HAS2-AS1 was hybridized with 20 nM digoxigenin-labeled HAS2-AS1 DNA probe at 4°C overnight and then detected with rhodamine-labeled antidigoxigenin antibody (Roche) after three washes. The cells were washed with PBS three times, incubated with 1% bovine serum albumin for 30 min, and then incubated with Alexa Fluor 488-conjugated EZH2 antibody at 4°C overnight. After 3 washes in washing buffer, cells were covered with 20 μL antifade reagent with 4′,6-diamidino-2-phenylindole (Vector Laboratories, Inc.) and sealed with coverslips by using mounting medium. Images were captured by confocal microscopy (Leica TCS SP8) at 400$\times$ magnification. The experiments were repeated independently at least three times, and representative images are shown.

Cell proliferation assay. The cells were transfected with EZH2 siRNAs or treated with DHZep for 48 h and then subjected to a cell viability assay using the CellTilter 96 Aqueous One solution cell proliferation assay (Promega Corporation), according to the manufacturer's instructions. The experiments were repeated independently at least three times, and representative results are shown.

Cell apoptosis assay. The cell apoptosis was evaluated by using a fluorescein isothiocyanate (FITC)-annexin V apoptosis detection kit with 7-aminoactinomycin D (7-AAD) (BioLegend). Cells were stained with FITC-labeled annexin V antibody and then incubated with 7-AAD for 10 min. Stained cells were analyzed using flow cytometry, and data were analyzed using Flowjo software (Ashland). The experiments were repeated independently at least three times, and representative results are shown.

Cell cycle analysis. The cells were fixed with 70% ethanol overnight at 4°C. The cells were washed with PBS twice and then treated with RNase A (0.5 mg/mL). The cells were stained with propidium iodide (5 mg/L) and then subjected to flow cytometry. The data were analyzed by Flowjo software (Ashland). The experiments were repeated independently at least three times and representative results are shown.

Antibodies. Antibodies (and their sources) used in this study included the following: mouse anti-HAS2 monoclonal antibody (Santa Cruz Biotechnology, Santa Cruz, CA, USA); mouse anti-GAPDH monoclonal antibody (Santa Cruz Biotechnology); rabbit anti-TGFβ1 antibody (Abcam, Cambridge, MA, USA); mouse anti-TGFβ2 monoclonal antibody (Abcam); rabbit anti-TGFβ3 polyclonal antibody (Abcam); rabbit anti-TGFBR1 polyclonal antibody (Abcam); rabbit anti-TGFBR2 monoclonal antibody (Abcam); rabbit anti-phospho-Akt (Ser473) polyclonal antibody (Cell Signaling Technology, Inc., MA, USA); rabbit anti-phospho-PI3K p85 (Tyr458) polyclonal antibody (Cell Signaling Technology); rabbit anti-PI3K p85 polyclonal antibody (Cell Signaling Technology); rabbit anti-Akt polyclonal antibody (Cell Signaling Technology); mouse anti-FOXO1 monoclonal antibody (Cell Signaling Technology); mouse anti-IκBα monoclonal antibody (Cell Signaling Technology); rabbit anti-Phospho-IκBα (Ser32) polyclonal antibody (Cell Signaling Technology); Alexa Fluor 488-conjugated mouse anti-EZH2 monoclonal antibody (Santa Cruz Biotechnology); mouse anti-SUZ12 monoclonal antibody (Santa Cruz Biotechnology); and rabbit anti-H3K27me3 monoclonal antibody (Abcam).

Statistical analysis. Statistical analysis was performed using SPSS software version 19.0 (IBM, Armonk, NY, USA). The HAS2-AS1 expression levels in patients and controls were evaluated with an unpaired *t* test. The cell migration, cell apoptosis, proliferation, and cell cycle data were analyzed with a paired *t* test. The differences between more than two groups were analyzed by one-way analysis of variance (ANOVA). The correlations between HAS2-AS1 expression and HAS2 protein level were analyzed by $\chi 2$ test. Two tailed $P < 0.05$ was considered to indicate a statistically significant difference.

Data availability. The data that support the findings of this study are available from the corresponding author, T.L., upon reasonable request.

ACKNOWLEDGMENTS

We are thankful for the support of the research center of The Second Affiliated Hospital of Zhengzhou University.

Conception and design, Y.X. and L.T.; data acquisition, Y.X., G.Y., Y.S., Y.L., L.C.; data analysis, Y.X.; funding acquisition, L.T.; resources, Y.X., G.Y., L.Z., M.W.; software, Y.X., G.Y.; writing—original draft, Y.X.; writing—review & editing, L.T.; final approval, Y.X., G.Y., Y.S., Y.L., L.C., P.L., L.Z., M.W., L.T.

This research was supported by The Education Department of Henan Province (182102311204).

We declare that we have no competing interests.

REFERENCES

1. Asuncion M, Calvo RM, San Millan JL, Sancho J, Avila S, Escobar-Morreale HF. 2000. A prospective study of the prevalence of the polycystic ovary syndrome in unselected Caucasian women from Spain. J Clin Endocrinol Metab 85:2434–2438. https://doi.org/10.1210/jc.85.7.2434.
2. Azziz R, Woods KS, Reyna R, Key TJ, Knochenhauer ES, Yildiz BO. 2004. The prevalence and features of the polycystic ovary syndrome in an unselected population. J Clin Endocrinol Metab 89:2745–2749. https://doi.org/10.1210/jc.2003-032046.
3. Goodarzi MO, Dumesic DA, Chazenbalk G, Azziz R. 2011. Polycystic ovary syndrome: etiology, pathogenesis and diagnosis. Nat Rev Endocrinol 7:219–231. https://doi.org/10.1038/nrendo.2010.217.
4. Das M, Djahanbakhch O, Hacihanefioglu B, Saridogan E, Ikram M, Ghali L, Raveendran M, Storey A. 2008. Granulosa cell survival and proliferation are altered in polycystic ovary syndrome. J Clin Endocrinol Metab 93:881–887. https://doi.org/10.1210/jc.2007-1650.
5. Song WJ, Shi X, Zhang J, Chen L, Fu SX, Ding YL. 2018. Akt-mTOR signaling mediates abnormalities in the proliferation and apoptosis of ovarian granulosa cells in patients with polycystic ovary syndrome. Gynecol Obstet Invest 83:124–132. https://doi.org/10.1159/000464351.
6. Homer MV, Rosencrantz MA, Shayya RF, Chang RJ. 2017. The effect of estradiol on granulosa cell responses to FSH in women with polycystic ovary syndrome. Reprod Biol Endocrinol 15:13. https://doi.org/10.1186/s12958-017-0230-0.
7. Erickson GF, Magoffin DA, Garzo VG, Cheung AP, Chang RJ. 1992. Granulosa cells of polycystic ovaries: are they normal or abnormal? Hum Reprod 7:293–299. https://doi.org/10.1093/oxfordjournals.humrep.a137638.
8. Shukla A, Dahiya S, Onteru SK, Singh D. 2018. Differentially expressed miRNA-210 during follicular-luteal transition regulates pre-ovulatory granulosa cell function targeting HRas and EFNA3. J Cell Biochem 119:7934–7943. https://doi.org/10.1002/jcb.26508.
9. Qin L, Huang CC, Yan XM, Wang Y, Li ZY, Wei XC. 2019. Long non-coding RNA H19 is associated with polycystic ovary syndrome in Chinese women: a preliminary study. Endocr J 66:587–595. https://doi.org/10.1507/endocrj.EJ19-0004.
10. Chao H, Spicer AP. 2005. Natural antisense mRNAs to hyaluronan synthase 2 inhibit hyaluronan biosynthesis and cell proliferation. J Biol Chem 280:27513–27522. https://doi.org/10.1074/jbc.M411544200.
11. Parnigoni A, Caon I, Moretto P, Viola M, Karousou E, Passi A, Vigetti D. 2021. The role of the multifaceted long non-coding RNAs: a nuclear-cytosolic interplay to regulate hyaluronan metabolism. Matrix Biol Plus 11:100060. https://doi.org/10.1016/j.mbplus.2021.100060.
12. Michael DR, Phillips AO, Krupa A, Martin J, Redman JE, Altaher A, Neville RD, Webber J, Kim MY, Bowen T. 2011. The human hyaluronan synthase 2 (HAS2) gene and its natural antisense RNA exhibit coordinated expression in the renal proximal tubular epithelial cell. J Biol Chem 286:19523–19532. https://doi.org/10.1074/jbc.M111.233916.
13. Vigetti D, Deleonibus S, Moretto P, Bowen T, Fischer JW, Grandoch M, Oberhuber A, Love DC, Hanover JA, Cinquetti R, Karousou E, Viola M,

D'Angelo ML, Hascall VC, De Luca G, Passi A. 2014. Natural antisense transcript for hyaluronan synthase 2 (HAS2-AS1) induces transcription of HAS2 via protein O-GlcNAcylation. J Biol Chem 289:28816–28826. https://doi.org/10.1074/jbc.M114.597401.
14. Yung Y, Ophir L, Yerushalmi GM, Baum M, Hourvitz A, Maman E. 2019. HAS2-AS1 is a novel LH/hCG target gene regulating HAS2 expression and enhancing cumulus cells migration. J Ovarian Res 12:21. https://doi.org/10.1186/s13048-019-0495-3.
15. Tong L, Wang Y, Ao Y, Sun X. 2019. CREB1 induced lncRNA HAS2-AS1 promotes epithelial ovarian cancer proliferation and invasion via the miR-466/RUNX2 axis. Biomed Pharmacother 115:108891. https://doi.org/10.1016/j.biopha.2019.108891.
16. Eldar-Geva T, Spitz IM, Groome NP, Margalioth EJ, Homburg R. 2001. Follistatin and activin A serum concentrations in obese and non-obese patients with polycystic ovary syndrome. Hum Reprod 16:2552–2556. https://doi.org/10.1093/humrep/16.12.2552.
17. Norman RJ, Milner CR, Groome NP, Robertson DM. 2001. Circulating follistatin concentrations are higher and activin concentrations are lower in polycystic ovarian syndrome. Hum Reprod 16:668–672. https://doi.org/10.1093/humrep/16.4.668.
18. Kolliopoulos C, Lin CY, Heldin CH, Moustakas A, Heldin P. 2019. Has2 natural antisense RNA and Hmga2 promote Has2 expression during TGFbeta-induced EMT in breast cancer. Matrix Biol 80:29–45. https://doi.org/10.1016/j.matbio.2018.09.002.
19. Zhao Z, Liang T, Feng S. 2019. Silencing of HAS2-AS1 mediates PI3K/AKT signaling pathway to inhibit cell proliferation, migration, and invasion in glioma. J Cell Biochem 120:11510–11516. https://doi.org/10.1002/jcb.28430.
20. Caon I, Bartolini B, Moretto P, Parnigoni A, Carava E, Vitale DL, Alaniz L, Viola M, Karousou E, De Luca G, Hascall VC, Passi A, Vigetti D. 2020. Sirtuin 1 reduces hyaluronan synthase 2 expression by inhibiting nuclear translocation of NF-kappaB and expression of the long-noncoding RNA HAS2-AS1. J Biol Chem 295:3485–3496. https://doi.org/10.1074/jbc.RA119.011982.
21. Li T, Mo H, Chen W, Li L, Xiao Y, Zhang J, Li X, Lu Y. 2017. Role of the PI3K-Akt signaling pathway in the pathogenesis of polycystic ovary syndrome. Reprod Sci 24:646–655. https://doi.org/10.1177/1933719116667606.
22. Liu M, Gao J, Zhang Y, Li P, Wang H, Ren X, Li C. 2015. Serum levels of TSP-1, NF-kappaB and TGF-beta1 in polycystic ovarian syndrome (PCOS) patients in northern China suggest PCOS is associated with chronic inflammation. Clin Endocrinol 83:913–922. https://doi.org/10.1111/cen.12951.
23. Rolaki A, Coukos G, Loutradis D, DeLisser HM, Coutifaris C, Makrigiannakis A. 2007. Luteogenic hormones act through a vascular endothelial growth factor-dependent mechanism to up-regulate alpha 5 beta 1 and alpha v beta 3 integrins, promoting the migration and survival of human luteinized granulosa cells. Am J Pathol 170:1561–1572. https://doi.org/10.2353/ajpath.2007.060926.
24. Franz MB, Daube S, Keck C, Sator M, Pietrowski D. 2013. Small GTPases are involved in sprout formation in human granulosa lutein cells. Arch Gynecol Obstet 287:819–824. https://doi.org/10.1007/s00404-012-2642-6.
25. Murai F, Koinuma D, Shinozaki-Ushiku A, Fukayama M, Miyaozono K, Ehata S. 2015. EZH2 promotes progression of small cell lung cancer by suppressing the TGF-beta-Smad-ASCL1 pathway. Cell Discov 1:15026. https://doi.org/10.1038/celldisc.2015.26.
26. Zhou H, Wu G, Ma X, Xiao J, Yu G, Yang C, Xu N, Zhang B, Zhou J, Ye Z, Wang Z. 2018. Attenuation of TGFBR2 expression and tumour progression in prostate cancer involve diverse hypoxia-regulated pathways. J Exp Clin Cancer Res 37:89. https://doi.org/10.1186/s13046-018-0764-9.
27. Long Y, Bolanos B, Gong L, Liu W, Goodrich KJ, Yang X, Chen S, Gooding AR, Maegley KA, Gajiwala KS, Brooun A, Cech TR, Liu X. 2017. Conserved RNA-binding specificity of polycomb repressive complex 2 is achieved by dispersed amino acid patches in EZH2. eLife 6. https://doi.org/10.7554/eLife.31558.
28. Kikin O, D'Antonio L, Bagga PS. 2006. QGRS Mapper: a web-based server for predicting G-quadruplexes in nucleotide sequences. Nucleic Acids Res 34:W676–W682. https://doi.org/10.1093/nar/gkl253.
29. Raja-Khan N, Kunselman AR, Demers LM, Ewens KG, Spielman RS, Legro RS. 2010. A variant in the fibrillin-3 gene is associated with TGF-beta and inhibin B levels in women with polycystic ovary syndrome. Fertil Steril 94:2916–2919. https://doi.org/10.1016/j.fertnstert.2010.05.047.
30. Urbanek M, Legro RS, Driscoll DA, Azziz R, Ehrmann DA, Norman RJ, Strauss JF, III, Spielman RS, Dunaif A. 1999. Thirty-seven candidate genes for polycystic ovary syndrome: strongest evidence for linkage is with follistatin. Proc Natl Acad Sci U S A 96:8573–8578. https://doi.org/10.1073/pnas.96.15.8573.
31. Li Y, Xiang Y, Song Y, Wan L, Yu G, Tan L. 2019. Dysregulated miR-142, -33b and -423 in granulosa cells target TGFBR1 and SMAD7: a possible role in polycystic ovary syndrome. Mol Hum Reprod 25:638–646. https://doi.org/10.1093/molehr/gaz014.
32. Parnigoni A, Caon I, Teo WX, Hua SH, Moretto P, Bartolini B, Viola M, Karousou E, Yip GW, Gotte M, Heldin P, Passi A, Vigetti D. 2022. The natural antisense transcript HAS2-AS1 regulates breast cancer cells aggressiveness independently from hyaluronan metabolism. Matrix Biol 109:140–161. https://doi.org/10.1016/j.matbio.2022.03.009.
33. Betancur JG, Tomari Y. 2015. Cryptic RNA-binding by PRC2 components EZH2 and SUZ12. RNA Biol 12:959–965. https://doi.org/10.1080/15476286.2015.1069463.
34. Rinn JL, Kertesz M, Wang JK, Squazzo SL, Xu X, Brugmann SA, Goodnough LH, Helms JA, Farnham PJ, Segal E, Chang HY. 2007. Functional demarcation of active and silent chromatin domains in human HOX loci by noncoding RNAs. Cell 129:1311–1323. https://doi.org/10.1016/j.cell.2007.05.022.
35. Zhao J, Sun BK, Erwin JA, Song JJ, Lee JT. 2008. Polycomb proteins targeted by a short repeat RNA to the mouse X chromosome. Science 322:750–756. https://doi.org/10.1126/science.1163045.
36. Klattenhoff CA, Scheuermann JC, Surface LE, Bradley RK, Fields PA, Steinhauser ML, Ding H, Butty VL, Torrey L, Haas S, Abo R, Tabebordbar M, Lee RT, Burge CB, Boyer LA. 2013. Braveheart, a long noncoding RNA required for cardiovascular lineage commitment. Cell 152:570–583. https://doi.org/10.1016/j.cell.2013.01.003.
37. Rotterdam ESHRE/ASRM-Sponsored PCOS Consensus Workshop Group. 2004. Revised 2003 consensus on diagnostic criteria and long-term health risks related to polycystic ovary syndrome. Fertil Steril 81:19–25. https://doi.org/10.1016/j.fertnstert.2003.10.004.
38. Hu Y, Lin J, Fang H, Fang J, Li C, Chen W, Liu S, Ondrejka S, Gong Z, Reu F, Maciejewski J, Yi Q, Zhao JJ. 2018. Targeting the MALAT1/PARP1/LIG3 complex induces DNA damage and apoptosis in multiple myeloma. Leukemia 32:2250–2262. https://doi.org/10.1038/s41375-018-0104-2.